Electronic Supplementary Information

Fe doped Ni-based oxalate framework with Favorable Electronic Structure for Electrocatalytic Water and Urea Oxidation

Chunzi Yang,[a,c] Ming Zhao,[a] Chunmei Zhang,[a] Shan Zhang,[a*] Dongdong Zhu,[b*] Chunxian Guo[a*]

[a] *School of Materials Science and Engineering, Suzhou University of Science and Technology, Suzhou 215009, China.*

E-mail: cxguo@usts.edu.cn, zs@usts.edu.cn

[b] *School of Chemistry and Materials Science, Institute of Advanced Materials and Flexible Electronics (IAMFE), Nanjing University of Information Science and Technology, Nanjing 210044, China.*

E-mail: dd.zhu@nuist.edu.cn

[c] *School of Environmental Science and Engineering, Suzhou University of Science and Technology, Suzhou 215009, China.*

1 Experimental Section

1.1 Chemicals and Reagents

Ferric nitrate nonahydrate ($Fe(NO_3)_3 \cdot 9H_2O$, AR, 98.5%), nickel nitrate hexahydrate ($Ni(NO_3)_2 \cdot 6H_2O$, AR, 98.5%) and oxalic acid ($C_2H_2O_4$, AR, 99%) were purchased from Greagent corporation. Ethanol (C_2H_5OH, AR, 99%), Hydrochloric acid (HCl, AR, 99%) and acetone (CH_3COCH_3, AR, 99%) were taken from Enox corporation. Potassium hydroxide (KOH, AR, 95%) were obtained from Aladdin corporation. Urea (CH_4N_2O, AR, 90%) was provided from Macklin corporation. Nickel foam (NF) was purchased from Shenzhen Green and Creative Environmental Science and Technology Co., Ltd and utilized as substrate. All chemicals were utilized as received without further purification and deionized water was obtained via Millipore system.

1.2 Synthesis

Synthesis of $Ni_xFe_{2-x}C_2O_4$: NF was cleaned successively with ethanol, acetone and 3.0 M HCl ultrasonic for 15 min, respectively, then washed with deionized water five times, and then dried at 60℃ for 12 h. The synthesis procedure of $Ni_xFe_{2-x}C_2O_4$ is based on previous literature[1] with some modification, where x represents amount of Ni-based precursor (mmol), and x=0, 0.2, 0.6, 1.4, 1.8, 2.0. Taking optimal $Ni_{0.6}Fe_{1.4}C_2O_4$ as an example, 0.6 mmol $Ni(NO_3)_2 \cdot 6H_2O$ and 1.4 mmol $Fe(NO_3)_2 \cdot 9H_2O$ were dissolved in 70 ml deionized water and stirred at 60℃ for 2 h to form solution A. 17.5 mmol anhydrous oxalic acid was mixed with 50 ml deionized water to form homogeneously solution B. Afterwards, solution B was slowly added to solution A using pipette to obtain uniform mixture. A piece of clean NF was placed into the mixture and kept at 60°C for 2 h. Then, NF covered with $Ni_{0.6}Fe_{1.4}C_2O_4$ was taken out and washed with ethanol and deionized water several times and dried overnight in an oven. Other samples with various Ni/Fe ratio were prepared through similar procedure except the amount of metal precursors. When single metal source is used, NiC_2O_4 (x=2.0) and FeC_2O_4 (x=0) can be obtained.

1.3 Characterization

Scanning electron microscopy (SEM) characterization was carried out on JSM-IT800SHL (JEOL, Japan) at the voltage of 10 kV. Transmission electron microscopy (TEM) and high-resolution TEM (HRTEM) images were obtained on JEM-F200 (Netherlands, 200 kV). X-ray photoelectron

spectroscopy (XPS) measurement was carried out on Thermo Fisher/ESCALAB Xi+ with Al Kα radiation. X-ray diffraction (XRD) patterns were performed on Bruker D8A A25.

1.4 Electrochemical measurements

All electrochemical tests were conducted on CHI 660D (Chenhua, Shanghai CH Instrument Inc) based on three-electrode system. The as-prepared $Ni_xFe_{2-x}C_2O_4$ with a surface area of 0.5 cm × 1 cm was applied as working electrode, while Pt plate and Ag/AgCl electrode are counter and reference electrode, respectively. The catalytic performance of $Ni_xFe_{2-x}C_2O_4$ was measured in 1 M KOH with or without 0.33 M urea. The linear sweep voltammetry (LSV) curves were measured from 1.0 V to 1.7 V *vs.* RHE at a scan rate of 5 $mV \cdot s^{-1}$. All LSV curves was corrected with 90% iR compensation, and all potentials were referred to Reversible Hydrogen Electrode (RHE) using the equation E(RHE)=E(Ag/AgCl) + 0.098 + 0.059 × pH. The Tafel slope is calculated from the Tafel equation ($\eta=b \log(j) + a$), where b is the Tafel slope ($mV\ dec^{-1}$). Electrochemical impedance spectroscopy (EIS) was carried out from 0.1 Hz to 100000 Hz. To calculate double-layer capacitance (C_{dl}), cyclic voltammetry (CV) curves were recorded with scan rates varied from 50 to 200 $mV\ s^{-1}$ in a non-faradaic potential window (1.175 V to 1.325 V *vs.* RHE). Then ECSA was calculated by dividing C_{dl} with the general specific capacitance for planar metal oxides (60 $\mu F\ cm^{-2}$)[2]. Chronoamperometric measurements were performed to evaluate the stability performance of $Ni_{0.6}Fe_{1.4}C_2O_4$. OER was performed at 1.463 V *vs.* RHE in the electrolyte of 1.0 M KOH, and UOR was measured at 1.368 V *vs.* RHE in 1.0 M KOH + 0.33 M urea. When measuring the stability for UOR, the electrolyte was refreshed for three times.

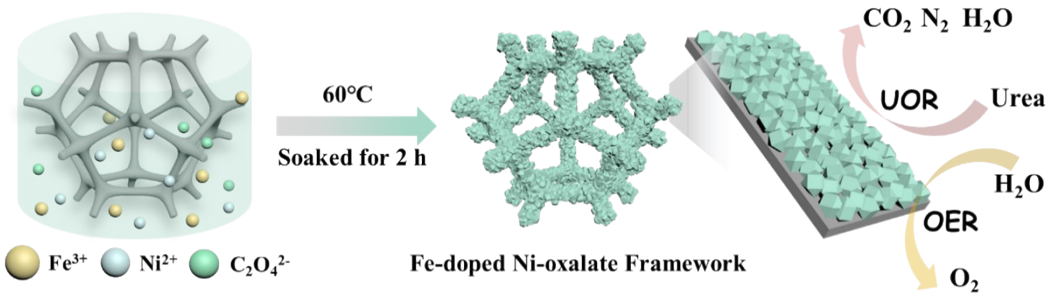

2 Supplementary Figures and Tables

Scheme1. Schematic illustration of the synthetic route for $Ni_xFe_{2-x}C_2O_4$.

Excessive oxalic acid holds the key to produce Fe doped Ni-based oxalate framework. As an organic weak acid, oxalic acid is able to etch NF surface, making the originally smooth surface uneven for favorable oxalate precipitation. On the other hand, oxalic acid can reduce Fe^{3+} to Fe^{2+}, along with some Fe^{2+} reduced by metal nickel, co-precipitating with Ni^{2+} to form Fe doped Ni-based oxalate framework. The deposited Fe doped Ni-based oxalate adheres to the NF surface, and prevents further etching of NF by oxalic acid.

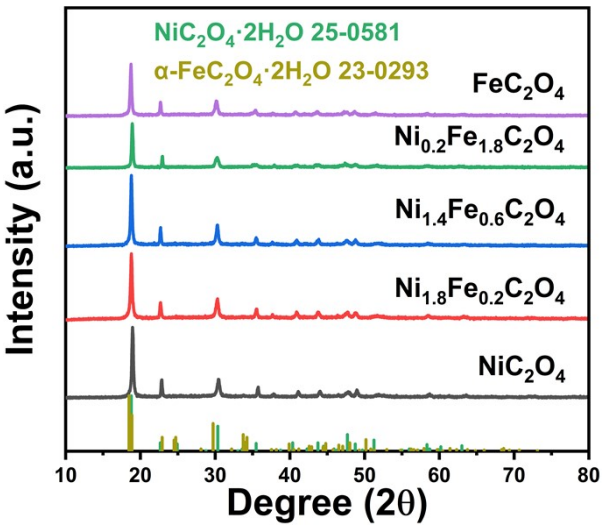

Figure S1. XRD patterns of a series of $Ni_xFe_{2-x}C_2O_4$ samples.

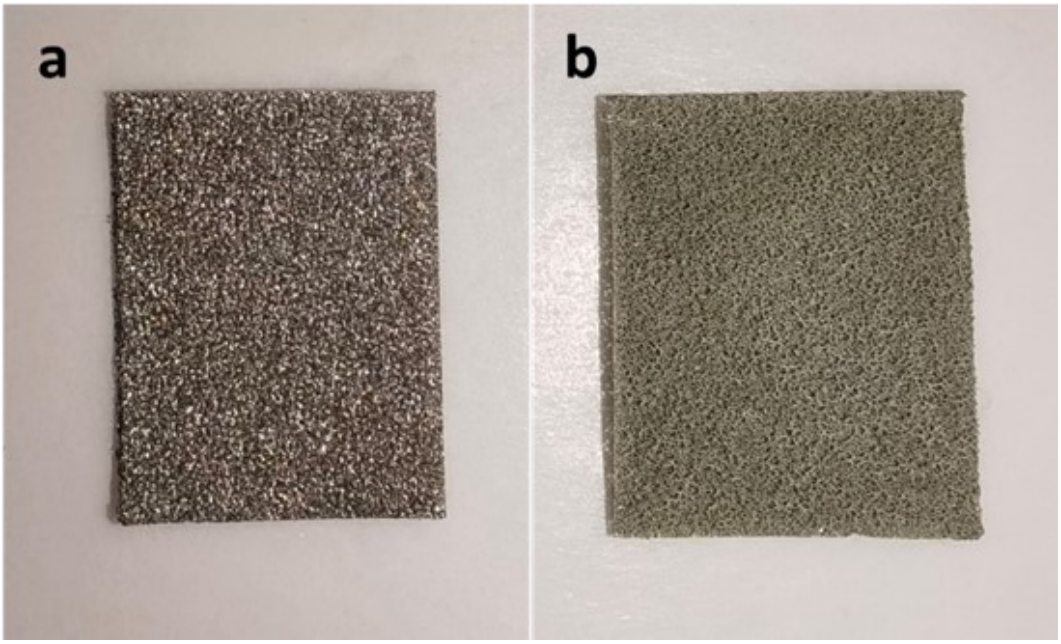

Figure S2. Optical images of (a) pre-treated NF and (b) $Ni_{0.6}Fe_{1.4}C_2O_4$ grown on NF.

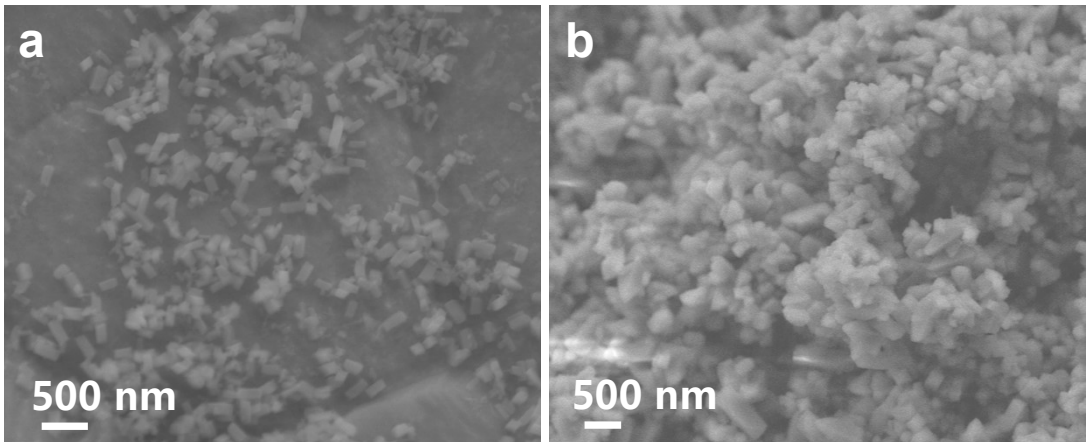

Figure S3. SEM images of (a) NiC_2O_4 and (b) FeC_2O_4.

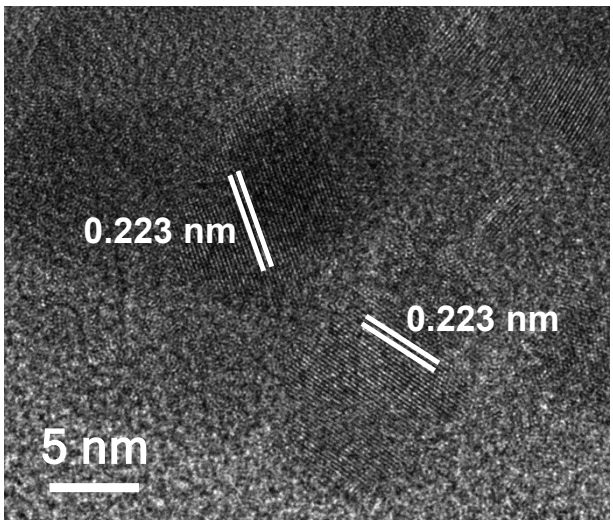

Figure S4. HRTEM image of $Ni_{0.6}Fe_{1.4}C_2O_4$.

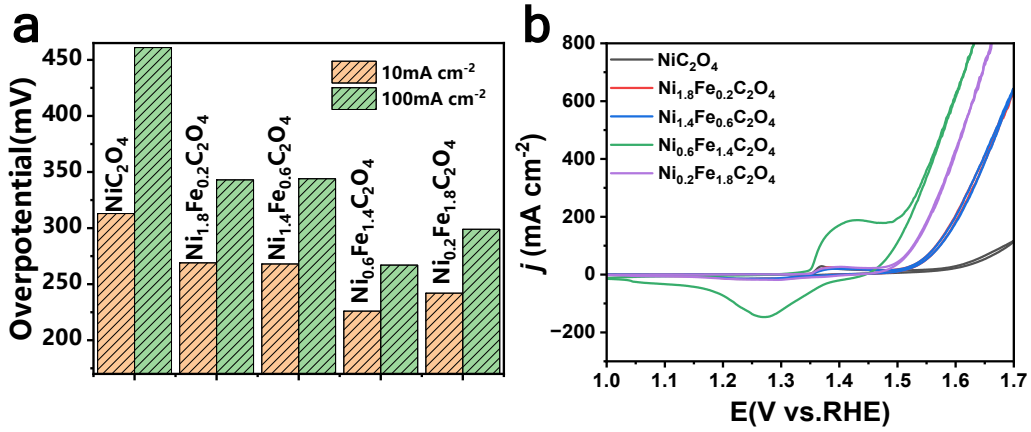

Figure S5. (a) η_{10} and η_{100} of different electrocatalysts for OER, (b) CV curves of $Ni_xFe_{2-x}C_2O_4$ in 1.0 M KOH.

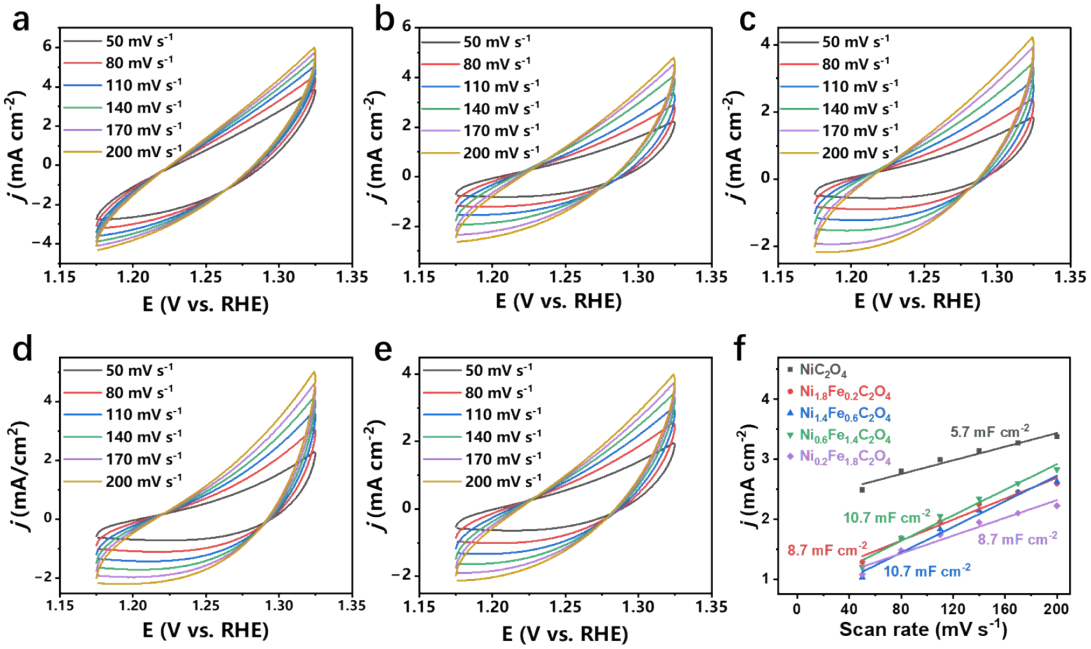

Figure S6. CV curves of $Ni_xFe_{2-x}C_2O_4$ samples with the scan rates from 50 to 200 mV s^{-1} in 1.0 M KOH: (a) NiC_2O_4, (b) $Ni_{1.8}Fe_{0.2}C_2O_4$, (c) $Ni_{1.4}Fe_{0.6}C_2O_4$, (d) $Ni_{0.6}Fe_{1.4}C_2O_4$, (e) $Ni_{0.2}Fe_{1.8}C_2O_4$, and (f) the corresponding C_{dl} values.

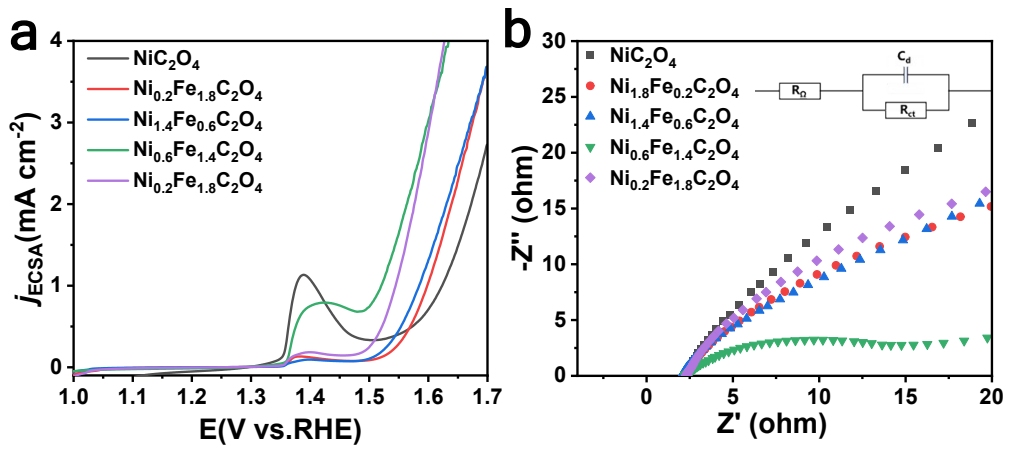

Figure S7. (a) ECSA-normalized LSV curves of $Ni_xFe_{2-x}C_2O_4$ in 1.0 M KOH, (b) Nyquist plots of $Ni_xFe_{2-x}C_2O_4$ in 1.0 M KOH.

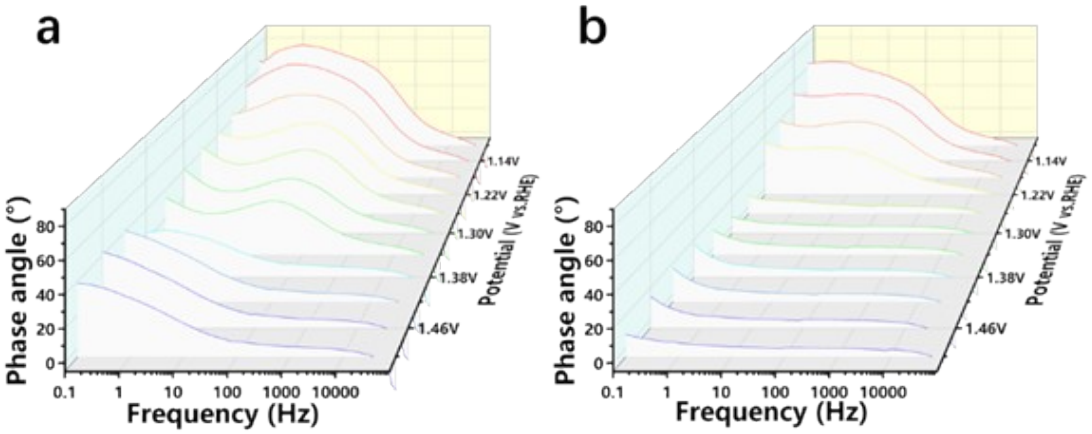

Figure S8. Bode plots of (a) NiC_2O_4, and (b) $Ni_{0.6}Fe_{1.4}C_2O_4$ in 1.0 M KOH.

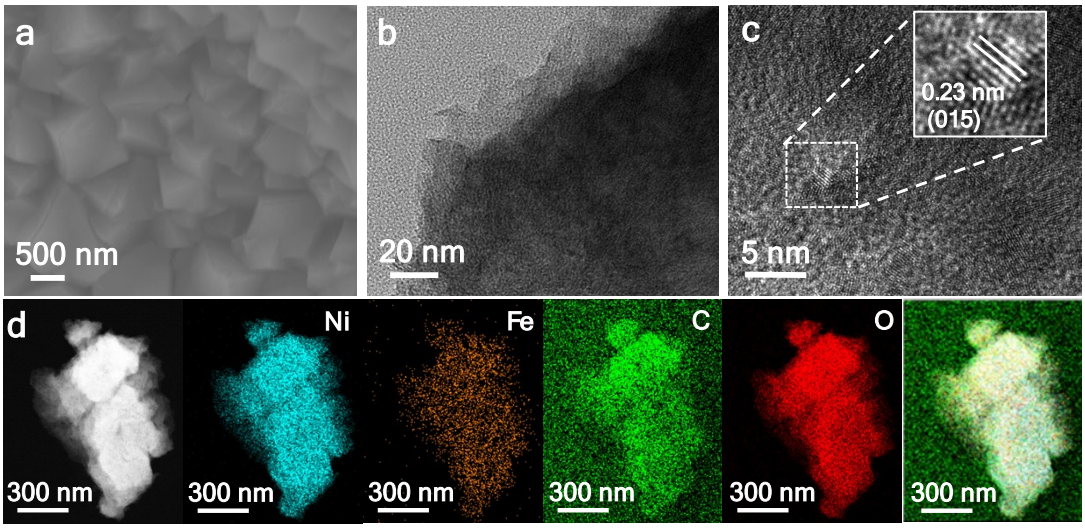

Figure S9. (a) SEM, (b) TEM and (c) HRTEM images of $Ni_{0.6}Fe_{1.4}C_2O_4$ after long-term OER stability test, (d) the corresponding EDX element mapping after OER stability test.

The lattice spacing of 0.23 nm in HRTEM image (Figure S9c) can be attributed to (015) plane of $Ni(OH)_2 \cdot 0.75H_2O$ (JCPDS No. 38-0715).

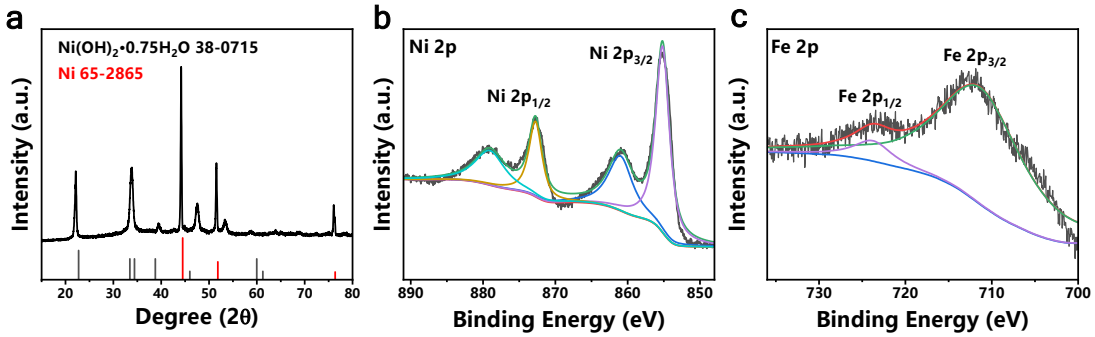

Figure S10. (a) XRD pattern of $Ni_{0.6}Fe_{1.4}C_2O_4$ electrocatalyst after long-term OER stability test, (b) Ni 2p and (c) Fe 2p XPS spectra of $Ni_{0.6}Fe_{1.4}C_2O_4$ after stability test.

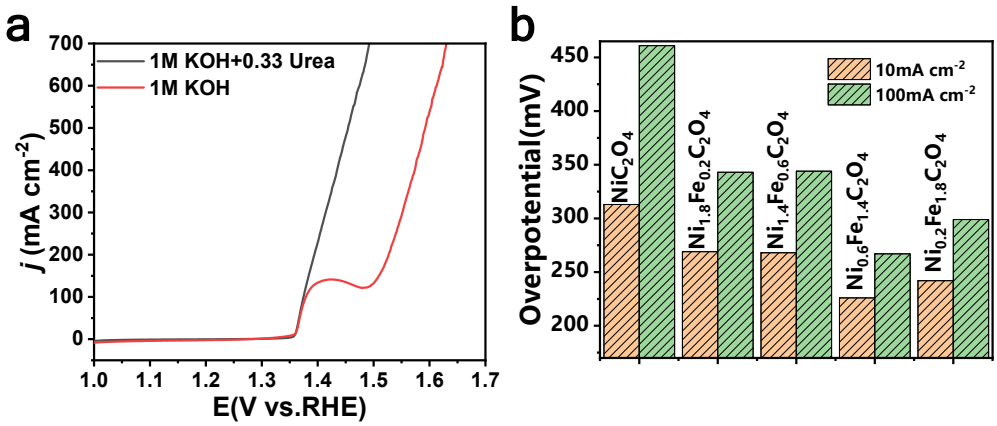

Figure S11. (a) LSV curves of $Ni_{0.6}Fe_{1.4}C_2O_4$ for OER and UOR; (b) η_{10} and η_{100} of $Ni_xFe_{2-x}C_2O_4$ samples for UOR.

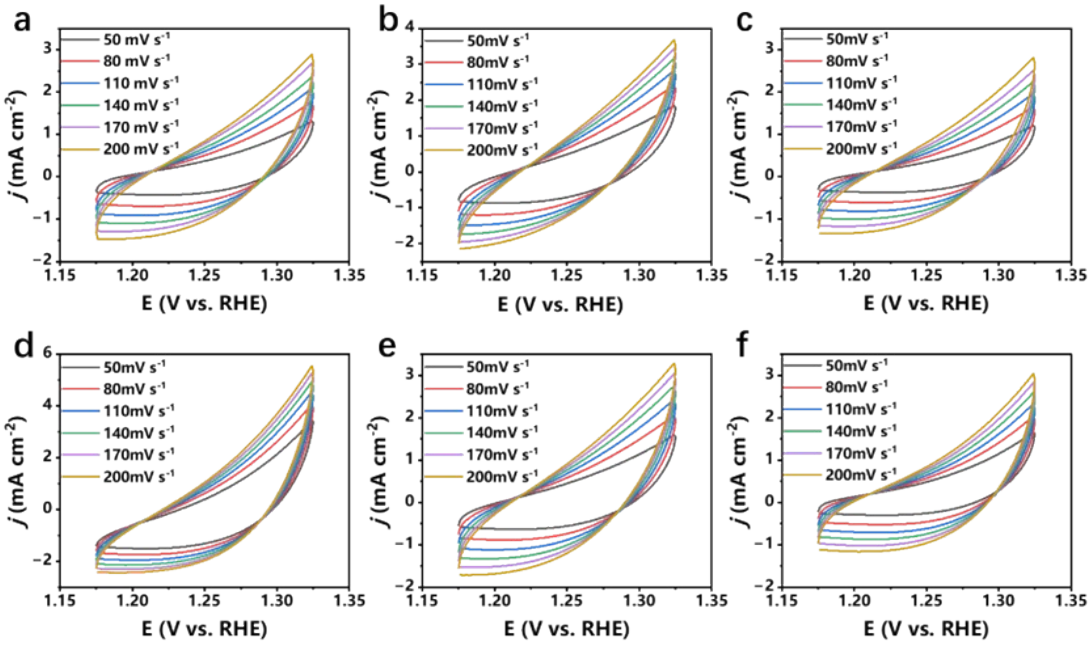

Figure S12. CV curves of $Ni_xFe_{2-x}C_2O_4$ with the scan rates from 50 to 200 mV s^{-1} in 1.0 M KOH and 0.33 M urea: (a) NiC_2O_4, (b) $Ni_{1.8}Fe_{0.2}C_2O_4$, (c) $Ni_{1.4}Fe_{0.6}C_2O_4$, (d) $Ni_{0.6}Fe_{1.4}C_2O_4$, (e) $Ni_{1.8}Fe_{0.2}C_2O_4$, and (f) FeC_2O_4.

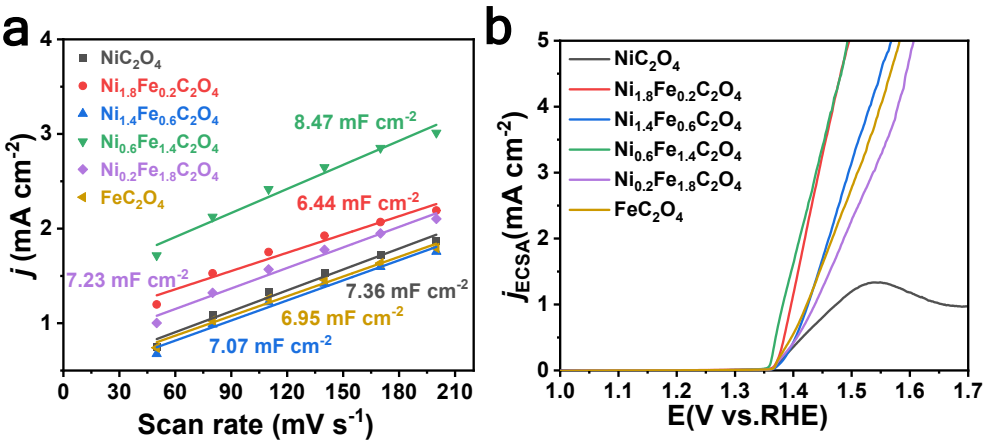

Figure S13. (a) C_{dl} values of $Ni_xFe_{2-x}C_2O_4$, and (b) ECSA-normalized LSV curves of $Ni_xFe_{2-x}C_2O_4$ in 1.0 M KOH and 0.33 M urea.

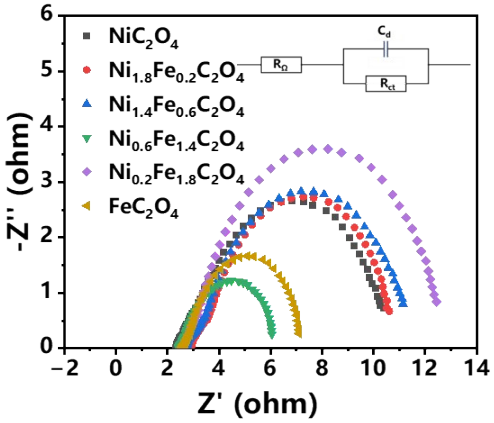

Figure S14. Nyquist plots of $Ni_xFe_{2-x}C_2O_4$ in 1.0 M KOH and 0.33 M urea.

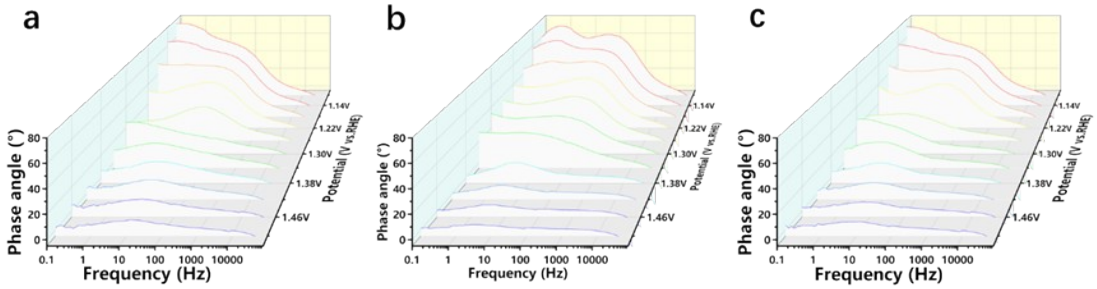

Figure S15. Bode plots of (a) NiC_2O_4, (b) $Ni_{0.6}Fe_{1.4}C_2O_4$ and (c) FeC_2O_4 in 1.0 M KOH and 0.33 M urea.

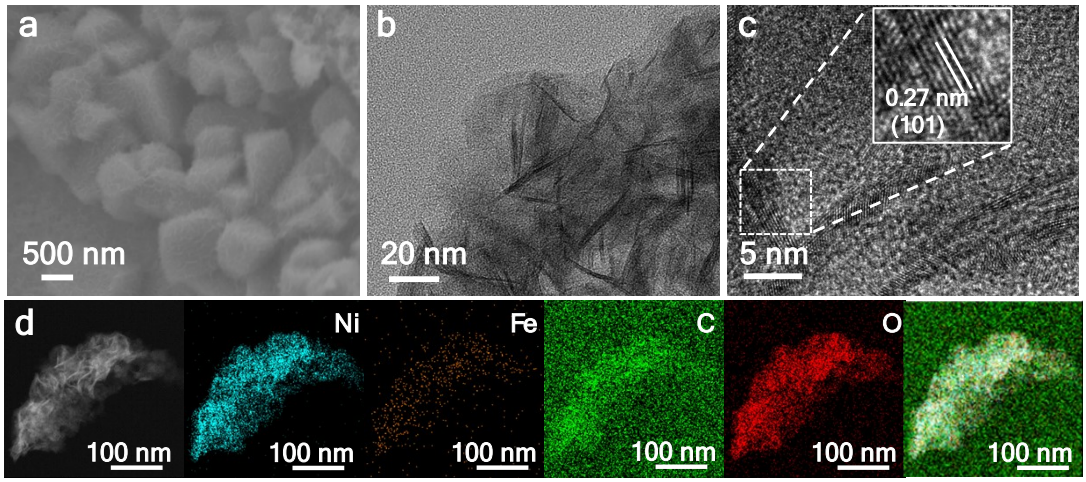

Figure S16. (a) SEM, (b) TEM and (c) HRTEM images of $Ni_{0.6}Fe_{1.4}C_2O_4$ after long-term UOR stability test, (d) the corresponding EDX element mapping after UOR stability test.

The lattice fringe of 0.27 nm in Figure S16c belongs to (101) plane of $Ni(OH)_2 \cdot 0.75H_2O$ (JCPDS No. 38-0715).

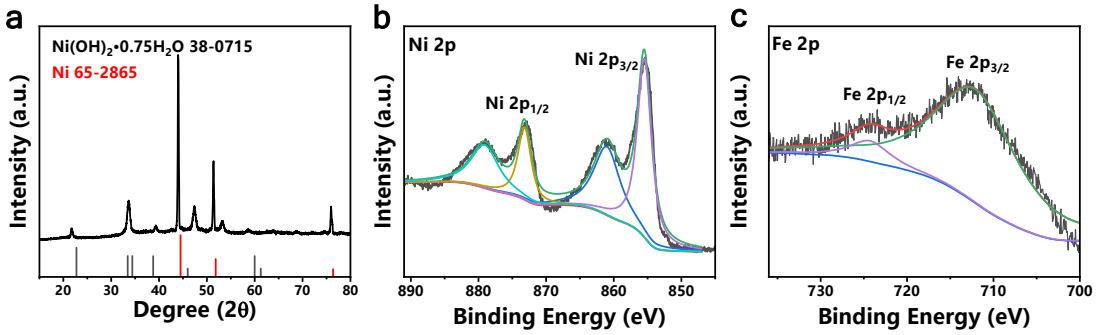

Figure S17. (a) XRD pattern of $Ni_{0.6}Fe_{1.4}C_2O_4$ electrocatalyst after long-term UOR stability test, (b) Ni 2p and (c) Fe 2p XPS spectra of $Ni_{0.6}Fe_{1.4}C_2O_4$ after UOR stability test.

Table S1. Comparison of OER performance of $Ni_{0.6}Fe_{1.4}C_2O_4$ with some recently reported electrocatalysts.

Catalysts	η_{100}/mV	Tafel Slope/ mV dec^{-1}	Reference
$Ni_{0.6}Fe_{1.4}C_2O_4$	267	22.63	This work
Ni/NMO	374	79.3	[3]
Fe-CoP/$Ni(OH)_2$	283	32	[4]
NiOOH/(LDH/α-FeOOH)	250	35	[5]
CoFeOF/NF	280	62.48	[6]
evo-FeOOH	>370	40.6	[7]
$NiCo_{1.75}Fe_{0.25}O_4$@NiO@NF	272	54	[8]
O-NFF	245	37.6	[2]
Fe(ox)$(H_2O)_2$/NF-(-1.4)-15	340	137	[9]
FeOOH/$NiCo_2S_4$/NF	256	62	[10]
Ni(Fe)OOH/Ni(Fe)Sx	274	32.4	[11]
NFF-AS_3	261	43.2	[12]
FMCO/NF	>289	52.1	[13]
B- $MnFe_2O_4$ @MFOC	298	87	[14]
C@CoP-FeP/FF	297	58.48	[15]

Table S2. Comparison of UOR performance of $Ni_{0.6}Fe_{1.4}C_2O_4$ with some recently reported electrocatalysts.

Catalysts	Urea concentration/M	Potential (V *vs.* RHE) for 100mA cm^{-2}	Tafel Slope/ mV dec^{-1}	Reference
$Ni_{0.6}Fe_{1.4}C_2O_4$	0.33	1.375	14.7	This work
Ni/NMO-10	0.5	1.43	51.2	[3]
O-NFF	0.33	1.42	12.1	[2]
NiOOH/(LDH/α-FeOOH)	0.33	1.40	30.1	[5]
Mo-NT@NF	0.33	1.46	31	[16]
W- NT@NF	0.33	1.43	94.8	[17]
$FeCoNiF_2$@NF	0.33	1.409	17	[18]
$Fe_xCo_{2-x}P$/ NF	0.5	1.39	33	[19]
NiF_3/ Ni_2P@CC-2	0.33	~1.53	33	[20]
[Fe_2P/Co_2P]@Mo_2S_3/NF	0.5	1.36	41.5	[21]
Ni/W_5N_4/NF	0.5	~1.4	35.8	[7]
LSFN-63	0.5	1.37	35	[22]
Ce-Ni_2P/NF	0.3	1.437	53.7	[23]
A-NiFeV/NF	0.33	1.39	34.8	[24]
Ni_3N/$Ni_{0.2}Mo_{0.8}N$/NF	0.5	1.366	17	[25]
ANH	0.33	1.34		[26]

References

1. S.-K. Geng, Y. Zheng, S.-Q. Li, H. Su, X. Zhao, J. Hu, H.-B. Shu, M. Jaroniec, P. Chen, Q.-H. Liu and S.-Z. Qiao, *Nat. Energy*, 2021, **6**, 904-912.
2. J. Kim, M. C. Kim, S. S. Han and K. Cho, *Adv. Funct. Mater.*, 2024, **34**, 2315625.
3. V. Maheskumar, A. Min, C. J. Moon, R. A. Senthil and M. Y. Choi, *Small Struct.*, 2023, **4**, 2300212
4. X. Yu, J. Zhao and M. Johnsson, *Adv. Funct. Mater.*, 2021, **31**, 2101578.
5. M. Cai, Q. Zhu, X. Wang, Z. Shao, L. Yao, H. Zeng, X. Wu, J. Chen, K. Huang and S. Feng, *Adv. Mater.*, 2022, **35**, 2209338
6. S. A. Patil, A. C. Khot, V. D. Chavan, I. Rabani, D.-k. Kim, J. Jung, H. Im and N. K. Shrestha, *Chem. Eng. J.*, 2024, **480**, 146545.
7. Y. Zhou, B. Chu, Z. Sun, L. Dong, F. Wang, B. Li, M. Fan and Z. Chen, *Appl. Catal. B-environ.*, 2023, **323**, 122168.
8. P. Upale, S. Verma and S. B. Ogale, *J. Mater. Chem. A*, 2023, **11**, 8972-8987.
9. Y. Hai, L. Liu and Y. Gong, *Inorg. Chem.*, 2021, **60**, 5140-5152.
10. M.-L. Guo, Z.-Y. Wu, M.-M. Zhang, Z.-J. Huang, K.-X. Zhang, B.-R. Wang and J.-C. Tu, *Rare Met.*, 2023, **42**, 1847-1857.
11. M. Chen, W. Li, Y. Lu, P. Qi, H. Wu, G. Liu, Y. Zhao and Y. Tang, *J. Mater. Chem. A*, 2023, **11**, 4608-4618.
12. S. Wu, Y. Zhu, G. Yang, H. Zhou, R. Li, S. Chen, H. Li, L. Li, O. Fontaine and J. Deng, *Chem. Eng. J.*, 2022, **446**, 136833.
13. W. Liu, W. Que, R. Yin, J. Dai, D. Zheng, J. Feng, X. Xu, F. Wu, W. Shi, X. Liu and X. Cao, *Appl. Catal. B-environ.*, 2023, **328**, 122488.
14. M. Chen, N. Kitiphatpiboon, C. Feng, Q. Zhao, A. Abudula, Y. Ma, K. Yan and G. Guan, *Appl. Catal. B-environ.*, 2023, **330**, 122577.
15. J. Li, Y. Hu, X. Huang, Y. Zhu and D. Wang, *Small*, 2023, **19**, 2206533
16. M. Liu, W. Zou, J. Cong, N. Su, S. Qiu and L. Hou, *Small*, 2023, **19**, 2302698.
17. M. Liu, W. Zou, S. Qiu, N. Su, J. Cong and L. Hou, *Adv. Funct. Mater.*, 2023, **34**, 2310155
18. N. T. Nguyen, T. T. N. Tran, T.-K. Truong, J. Yu, T. N.-M. Le, T. B. Phan, T. L. H. Doan, L. H. T. Nguyen, T. D. Luong, T.-H. Nguyen and N. Q. Tran, *Inorg. Chem.*, 2023, **62**, 10298-10306.

19. T. I. Singh, G. Rajeshkhanna, S. B. Singh, T. Kshetri, N. H. Kim and J. H. Lee, *ChemSusChem*, 2019, **12**, 4810-4823.
20. K. Wang, W. Huang, Q. Cao, Y. Zhao, X. Sun, R. Ding, W. Lin, E. Liu and P. Gao, *Chem. Eng. J.*, 2022, **427**, 130865.
21. L. Wang, W. He, D. Yin, Y. Xie, H. Zhang, Q. Ma, W. Yu, Y. Yang and X. Dong, *Chem. Eng. J.*, 2023, **462**, 142254.
22. Y. Gan, Y. Ye, X. Dai, X. Yin, Y. Cao, R. Cai, B. Feng, Q. Wang and X. Zhang, *Small*, 2023, **19**, 2303250.
23. K. Xiong, L. Yu, Y. Xiang, H. Zhang, J. Chen and Y. Gao, *J. Alloys Compd.*, 2022, **912**, 165234.
24. H. Yang, L. Ge, J. Guan, B. Ouyang, H. Li and Y. Deng, *J. Colloid Interface Sci.*, 2024, **653**, 721-729.
25. R.-Q. Li, X.-Y. Wan, B.-L. Chen, R.-Y. Cao, Q.-H. Ji, J. Deng, K.-G. Qu, X.-B. Wang and Y.-C. Zhu, *Chem. Eng. J.*, 2021, **409**, 128240.
26. Y. Zhu, C. Liu, S. Cui, Z. Lu, J. Ye, Y. Wen, W. Shi, X. Huang, L. Xue, J. Bian, Y. Li, Y. Xu and B. Zhang, *Adv. Mater.*, 2023, **35**, 2301549.